M(H2O)(PO3C10H6OH)×(H2O)0.5 (M = Co, Mn, Zn, Cu): a new series of layered metallophosphonate compoundsobtained from 6-hydroxy-2-naphthylphosphonic acid

Felicien Beaubras, Jean-Michel Rueff, Olivier Perez, Fabien Veillon, Vincent Caignaert, Lohier Jean-François, Julien Cardin, Guillaume Rogez, Charlotte Jestin, Hélène Couthon, et al.

$M(H_2O)(PO_3C_{10}H_6OH)\cdot(H_2O)_{0.5}$ (M = Co, Mn, Zn, Cu): a new series of layered metallophosphonate compounds obtained from 6-hydroxy-2-naphthylphosphonic acid†

Félicien Beaubras,[a] Jean-Michel Rueff, *[a] Olivier Perez,[a] Fabien Veillon,[a] Vincent Caignaert,[a] Jean-François Lohier,[b] Julien Cardin,[c] Guillaume Rogez,[d] Charlotte Jestin,[e] Hélène Couthon[e] and Paul-Alain Jaffrès *[e]

Four new metallophosphonates $M(H_2O)(PO_3C_{10}H_6OH)\cdot(H_2O)_{0.5}$ (M = Mn, Co, Cu, Zn) were obtained as single crystal and polycrystalline powders by hydrothermal synthesis from the precursors 6-hydroxy-2-naphthylphosphonic acid and the corresponding metal salts. These analogous hybrids crystalized in the space group $P12_1/c1$ in a lamellar structure. Their layered structures consisted of inorganic [$M(H_2O)(PO_3C)$] layers stacked with organic bilayers of 6-hydroxy-2-naphthyl moieties "$HO-C_{10}H_6$" and free water molecules. Their structures were determined by single crystal X-ray diffraction and confirmed by powder X-ray diffraction and Le Bail refinement for the powder sample. The removal of water upon heating at 250 °C was studied by thermogravimetric analysis and temperature-dependent powder X-ray diffraction. Their magnetic properties were studied by SQUID magnetometry and show antiferromagnetic behavior for the Co analogue and the occurrence of a canted antiferromagnetic order at T_N = 12.2 K for the Mn analogue. The Cu compound displayed an unprecedented ferromagnetic behavior. Their absorption and luminescence properties were investigated and revealed that the ligand and the compounds displayed a common behavior below a wavelength of 400 nm. Specific absorption bands were found in the compounds with Co^{2+} and Cu^{2+} at 539 nm and 849 nm, respectively. Moreover, particular luminescence bands were found for the compounds with Mn^{2+}, Co^{2+} and Zn^{2+} at 598 nm, 551 nm and 530 and 611 nm, respectively.

Introduction

Since the pioneering work of A. Clearfield who reported the crystal structure and exchange properties of zirconium-phosphate,[1] and subsequently the works of Alberti[2] and Clearfield[3,4] who reported the preparation of metal-phosphonate hybrids that are synthesized from phosphonic acids,[5–7] many crystalline hybrid materials belonging to this class of materials have been reported. They were prepared by using different synthesis conditions including hydrothermal,[8,9] solvothermal,[10,11] ionothermal[12] or mechanosynthesis[13] and by using phosphonic acid,[14] phosphonate[15] or phosphonic acid monoester[16] as organic substrates. One of the first metal-phosphonates that was reported (zirconium-phenylphosphonate) possessed a layered structure with the organic moieties located within the interlayer space.[2] The development of materials featuring new properties resulted from a rational choice of both organic and metal precursors.[17] The functionalization of the organic moieties allowed the introduction of new properties including coordination properties used for catalysis[18,19] and asymmetric catalysis,[20] ionic conduction,[21] and fluorescence[22] or the preparation of microporous[23] or mesoporous[24] materials. On the other hand, a rational selection of the metal ions offered properties like magnetism,[25,26] luminescence,[27–29] bactericidal action[30] or controlled metallic salt release.[31] In our laboratories, we developed a strategy that consisted of preparing rigid phosphonic acids[32] possessing a low symmetry[33] with the aim of synthesiz-

[a]Normandie Univ, ENSICAEN, UNICAEN, CNRS, CRISMAT, 6 Bd Maréchal Juin, 14050 Caen Cedex, France. E-mail: jean-michel.rueff@ensicaen.fr
[b]Normandie Univ, ENSICAEN, UNICAEN, CNRS, LCMT, 6 Bd Maréchal Juin, 14050 Caen Cedex, France
[c]Normandie Univ, ENSICAEN, UNICAEN, CNRS, CIMAP, 6 Bd Maréchal Juin, 14050 Caen Cedex, France
[d]IPCMS, UMR Unistra-CNRS 7504, 23 rue du Loess, BP 43, 67034 Strasbourg Cedex 2, France
[e]Univ Brest, CEMCA UMR CNRS 6521, 6 Avenue Victor Le Gorgeu, 29238 Brest, France. E-mail: Paul-Alain.Jaffres@univ-brest.fr

†Electronic supplementary information (ESI) available. CCDC 1956355–1956357 contains the supplementary crystallographic data for this paper. For ESI and crystallographic data in CIF or other electronic format see DOI: 10.1039/C9DT03947C

ing non-centrosymmetric metal-phosphonate hybrids as a prerequisite for producing materials featuring multiferroic properties.[34,35] In a few cases, magneto-electric coupling was observed.[36–38] Since the properties of hybrid materials are influenced by the functionalization of organic precursors and after considering the incorporation of carboxylic acids[9] or halogen atoms into organic precursors[38,39] in addition to one or several phosphonic acid functions,[40] we investigate herein the conception of metal-phosphonate hybrids featuring phenol functions. Actually, only a few metal-phosphonate materials possessing phenol functions were previously reported in the literature. A first example used 2,5-dihydroxy-1,4-benzenediphosphonic acid as a ligand to prepare uranyl-organic hybrids.[41] The same organic precursor was used in association with zinc(II) to produce a three-dimensional hybrid featuring microporosity.[42] In both cases, the phenol functions were not coordinated to the inorganic network. In addition to these crystalline materials, an amorphous hybrid featuring phenol functions was prepared from binaphthol di-phosphonic acids as organic precursors. This hybrid material was used as a chiral catalyst for the addition of diethylzinc on aromatic aldehyde.[43] The incorporation of phenol functions in the structures of metal phosphonates could modify their properties in different ways. First, phenol functions can be involved in an hydrogen bonding network that could stabilize the final hybrid material or that could produce ionic conduction properties. Phenol functions can also act as ligands and could participate in inorganic networks. Phenol and naphthol could present fluorescence properties as recently reported for a naphthyl phosphonic derivative.[22] Finally, phenol functions could allow the post functionalization of hybrid materials (*e.g.* reaction with diazonium salts) or could feature proton exchange properties due to their acidity ($pK_a \approx 9$). All these possible properties make the preparation of new metal-phosphonate hybrids possessing phenol functions interesting. Herein we report the synthesis, structure and properties (magnetism and photoluminescence) of four metal-phosphonates that were prepared under hydrothermal conditions from 6-hydroxy-2-naphthalenephosphonic acid **2** and a selected metal salt M^{2+} (Mn^{2+}, Co^{2+}, Cu^{2+}, Zn^{2+}). The magnetic properties were investigated by SQUID magnetometry and an overall antiferromagnetic behavior for the Co and Mn analogues was observed, with the occurrence of a canted antiferromagnetic order at T_N = 12.2 K for the Mn analogue. The Cu compound displayed unprecedented ferromagnetic behavior. Numerous investigations of organic compounds with photoluminescence (PL) properties have been carried out in the last two decades with the perspective of developing new organic based optoelectronic technologies, as for example organic light-emitting diodes (OLEDs). However, the applicability of these organic materials is limited by the difficulty of controlling the distances between the aryl molecules, their relative orientations and by the lack of thermal stability and rigidity of their frameworks. An attractive way to produce new photoluminescence properties is to associate a conjugated organic group with a transition element, as nicely shown for the large family of metal–organic frameworks (MOFs).[27] In this perspective, the d–d transition-metal complexes containing aryl ligands studied more than thirty years ago[44–46] represent a huge source of new luminescence features/properties with high stability compared to other hybrids.

The Zn^{2+} ion with a $3d^{10}$ electronic configuration does allow any possible transition resulting in no Zn^{2+} related absorption bands, yielding a colorless product. The Mn^{2+}, Co^{2+} and Cu^{2+} ions with the electronic configurations of $3d^5$, $3d^7$ and $3d^9$ respectively present strictly forbidden d–d intraconfigurational transitions that are weakly allowed by inter-configurational mixing through odd-parity crystal fields and vibrations.[47] In the octahedral crystal field imposed by the structures of our compounds, they exhibit spin allowed transition bands to the ground state resulting in colored compounds. Mn^{2+} is predicted to have a large number of energy levels (252) with overlapping, allowing transitions to the ground state and resulting in a brown-pink colored compound.[48] Co^{2+} is predicted to have a large number of energy levels (120) with spin allowed transitions to the ground state resulting in a purple pink colored compound.[49,50] Cu^{2+} is predicted to have fewer energy levels (10) with spin allowed transitions to the ground state resulting in a green-blue colored compound.

Experimental

All reagents were used as received and without further purification. Manganese nitrate tetrahydrate ($Mn(NO_3)_2{\cdot}4H_2O$, ≥98%), cobalt nitrate hexahydrate ($Co(NO_3)_2{\cdot}4H_2O$, ≥98%), copper sulphate pentahydrate ($CuSO_4{\cdot}5H_2O$, ≥98%) and zinc nitrate hexahydrate ($Zn(NO_3)_2{\cdot}6H_2O$, ≥98%) were purchased from Sigma Aldrich, Alpha Aesar and Merck. Diethyl 6-hydroxy-2-naphthylphosphonate (**1**) and 6-hydroxy-2-naphthylphosphonic acid (**2**) were prepared by adapting the reported methods (details in ESI 1†). Hydrothermal syntheses were performed by using Berghof DAB-2 pressure digestion vessels. Elemental analyses were performed with an automatic CHNS-O Thermo-Quest NA 2500 apparatus. Thermogravimetric analyses (TGA) were performed in alumina crucibles under air at the rate of 2 °C min^{-1} from room temperature to 1000 °C on polycrystalline samples by using a SETARAM Setsys evolution apparatus. The selection of single crystal platelets for single crystal X-ray diffraction was performed using a polarizing Zeiss discovery V20 stereo-microscope. The crystal structures of the compounds were solved with either Superflip[51] using charge flipping[52] and refined with Jana2006[53] or Olex 2[54] software using shelX office. Powder X-ray diffraction patterns were recorded with a laboratory (i) Philips X'PERT Pro MPD PANalytical diffractometer equipped with an X'celerator detector and (ii) with a laboratory Bruker D8 advance diffractometer using monochromated Cu-Kα1 radiation ($\lambda_{K\alpha1}$ = 1.5406 Å) and a LynxEye detector. Temperature powder X-ray diffraction patterns were recorded with a laboratory Bruker D8 advance diffractometer using

monochromated Cu-Kα1 radiation ($\lambda_{K\alpha1}$ = 1.5406 Å), equipped with a LynxEye detector and an Anton Paar HTK1200N temperature chamber. Le Bail refinements were performed to confirm the purity of the powder samples. The magnetic studies were carried out with a SQUID magnetometer (Quantum Design MPMS-XL) covering the temperature and field ranges of 2–300 K and ±5 T, respectively. Magnetization *vs.* field measurements at room temperature confirm the absence of ferromagnetic impurities. Data were corrected for the sample holder and diamagnetism was estimated from Pascal constants. The absorbance spectra were obtained using a PerkinElmer Lambda 1050 UV/Vis spectrophotometer with 150 mm integrating spheres in total transmittance mode in normal incidence. In order to carry out the spectroscopy experiments, the powdered compounds were positioned between two Suprasil™ glass slides from Hellma Analytics. The continuous wave (CW) photoluminescence (PL) measurements were carried out at room temperature using a Crylas FQCW266 excitation laser emitting at 266 nm with an average power of 27 mW, with an incident angle of 45° on a beam spot size of about 1 mm^2 and chopped at 3.00 Hz for the samples. Emitted photons were collected into a light cone of 28° by means of a set of lenses and a Horiba Jobin-Yvon Triax 180 monochromator. An R5108 Hamamatsu photomultiplier tube connected to a SR830 lock-in amplifier referenced at the excitation light chopper frequency ensured detection. The samples of PL spectra were measured on powder stacked between two quartz Suprasil™ glass slides purchased from Hellma Analytics.

Hydrothermal synthesis of the hybrid materials

$Mn(H_2O)(PO_3C_{10}H_6OH)\cdot(H_2O)_{0.5}$ (**3**), $Co(H_2O)(PO_3C_{10}H_6OH)\cdot(H_2O)_{0.5}$ (**4**), $Cu(H_2O)(PO_3C_{10}H_6OH)\cdot(H_2O)_{0.5}$ (**5**) and $Zn(H_2O)(PO_3C_{10}H_6OH)\cdot(H_2O)_{0.5}$ (**6**) hybrid materials were synthesized by a hydrothermal method according to the following procedures:

$Mn(H_2O)(PO_3C_{10}H_6OH)\cdot(H_2O)_{0.5}$ (3). A 50 mL PTFE liner was charged with a mixture of 6-hydroxy-2-naphthylphosphonic acid (**2**) (0.05 g, 0.22 mmol, 1 eq.), manganese nitrate tetrahydrate $Mn(NO_3)_2\cdot4H_2O$ (0.083 g, 0.33 mmol, 1.5 eq.), urea (0.013 g, 0.22 mmol, 1 eq.) and distilled water (10 mL). The liner was then inserted in a Berghof DAB-2 pressure digestion vessel and heated from room temperature to 120 °C in 24 hours, left at 120 °C for 24 hours and cooled to room temperature in 24 hours. The final compound was obtained after filtration as platelet light brown crystals which were washed with distilled water, rinsed with ethanol and dried in air (quantity 35.6 mg; yield 71%). Elemental analysis for $MnC_{10}PO_{5.5}H_{10}$ (304.1 g mol^{-1}): found (calc.) C 39.99% (39.49), H 3.88% (3.31).

$Co(H_2O)(PO_3C_{10}H_6OH)\cdot(H_2O)_{0.5}$ (4). A 50 mL PTFE liner was charged with a mixture of 6-hydroxy-2-naphthylphosphonic acid (**2**) (0.05 g, 0.22 mmol, 1 eq.), cobalt nitrate hexahydrate $Co(NO_3)_2\cdot4H_2O$ (0.097 g, 0.33 mmol, 1.5 eq.), urea (0.013 g, 0.22 mmol, 1 eq.) and distilled water (10 mL). The liner was then inserted into a Berghoff DAB-2 pressure digestion vessel and heated from room temperature to 130 °C in 24 hours, left at 130 °C for 36 hours and cooled to room temperature in 24 hours. The final compound was obtained after filtration as clear light violet platelet crystals which were washed with distilled water, rinsed with ethanol and dried in air (quantity 41.5 mg; yield 83%). Elemental analysis for $CoC_{10}PO_{5.5}H_{10}$ (308.08 g mol^{-1}): found (calc.) C 39.80% (38.98%), H 4.24% (3.27%).

$Cu(H_2O)(PO_3C_{10}H_6OH)\cdot(H_2O)_{0.5}$ (5). A 50 mL PTFE liner was charged with a mixture of 6-hydroxy-2-naphthylphosphonic acid (**2**) (0.05 g, 0.22 mmol, 1 eq.), copper sulphate pentahydrate $CuSO_4\cdot5H_2O$ (0.082 g, 0.33 mmol, 1.5 eq.) and distilled water (10 mL). The liner was then inserted into a Berghoff DAB-2 pressure digestion vessel and heated from room temperature to 110 °C in 12 hours, left at 120 °C for 24 hours and cooled to room temperature in 36 hours. The final compound was obtained after filtration as platelet green crystals, which were washed with distilled water, rinsed with ethanol and dried in air (quantity 26.5 mg; yield 53%). Elemental analysis for $CuC_{10}PO_{5.5}H_{10}$ (312.7 g mol^{-1}): found (calc.) C 39.43% (38.41%), H 3.93% (3.22%).

$Zn(H_2O)(PO_3C_{10}H_6OH)\cdot(H_2O)_{0.5}$ (6). A 50 mL PTFE liner was charged with an equimolar mixture of 6-hydroxy-2-naphthylphosphonic acid (**2**) (0.05 g, 0.22 mmol, 1 eq.), zinc nitrate hexahydrate $Zn(NO_3)_2\cdot6H_2O$ (0.066 g, 0.22 mmol, 1 eq.), urea (0.013 g, 0.22 mmol, 1 eq.) and distilled water (10 mL). The liner was then inserted into a Berghoff DAB-2 pressure digestion vessel and heated from room temperature to 140 °C in 24 hours, left at 140 °C for 24 hours and cooled to room temperature in 24 hours. The final compound was obtained after filtration as platelet colorless crystals that were washed with distilled water, rinsed with ethanol and dried in air (quantity 19.5 mg; yield 65%). Elemental analysis for $ZnC_{10}PO_{5.5}H_{10}$ (314.54 g mol^{-1}): found (calc.) C 38.39% (38.18%), H 3.80% (3.20%).

Soft chemistry synthesis in a round bottom flask

$Mn(H_2O)(PO_3C_{10}H_6OH)\cdot(H_2O)_{0.5}$ (**3**), $Co(H_2O)(PO_3C_{10}H_6OH)\cdot(H_2O)_{0.5}$ (**4**), $Cu(H_2O)(PO_3C_{10}H_6OH)\cdot(H_2O)_{0.5}$ (**5**) and $Zn(H_2O)(PO_3C_{10}H_6OH)\cdot(H_2O)_{0.5}$ (**6**) hybrid materials were synthesized by a soft chemistry method according to the following procedure:

$Mn(H_2O)(PO_3C_{10}H_6OH)\cdot(H_2O)_{0.5}$ (3). A 250 mL round-bottom flask was charged with a mixture of 6-hydroxy-2-naphthylphosphonic acid (**2**) (0.03 g, 0.13 mmol, 1 eq.), manganese nitrate tetrahydrate $Mn(NO_3)_2\cdot4H_2O$ (0.050 g, 0.2 mmol, 1.5 eq.), urea (0.008 g, 0.13 mmol, 1 eq.) and distilled water (25 mL). The solution was stirred and heated at 130 °C and left at this temperature for 4 hours and cooled to room temperature. The final compound was isolated after filtration as light brown powder that was washed with distilled water, rinsed with ethanol and dried in air (quantity 21.6 mg; yield 72%).

$Co(H_2O)(PO_3C_{10}H_6OH)\cdot(H_2O)_{0.5}$ (4). A 250 mL round-bottom flask was charged with a mixture of 6-hydroxy-2-naphthylphosphonic acid (**2**) (0.03 g, 0.13 mmol, 1 eq.), cobalt nitrate hexa-

hydrate $Co(NO_3)_2{\cdot}4H_2O$ (0.058 g, 0.2 mmol, 1.5 eq.), urea (0.008 g, 0.13 mmol, 1 eq.) and distilled water (25 mL). The solution was stirred and heated at 140 °C, left at this temperature for 4 hours and cooled to room temperature. The final compound was obtained after filtration as a light violet powder that was washed with distilled water, rinsed with ethanol and dried in air (quantity 23.4 mg; yield 78%).

$Cu(H_2O)(PO_3C_{10}H_6OH){\cdot}(H_2O)_{0.5}$ (5). A 250 mL round-bottom flask was charged with a mixture of 6-hydroxy-2-naphthylphosphonic acid (**2**) (0.03 g, 0.13 mmol, 1 eq.), copper sulphate pentahydrate $CuSO_4{\cdot}5H_2O$ (0.050 g, 0.2 mmol, 1.5 eq.) and distilled water (25 mL). The solution was stirred and heated at 120 °C, left at this temperature for 4 hours and cooled to room temperature. The final compound was obtained after filtration as a light green powder that was washed with distilled water, rinsed with ethanol and dried in air (quantity 19.5 mg; yield 65%).

$Zn(H_2O)(PO_3C_{10}H_6OH){\cdot}(H_2O)_{0.5}$ (6). A 250 mL round-bottom flask was charged with a mixture of 6-hydroxy-2-naphthylphosphonic acid (**2**) (0.03 g, 0.13 mmol, 1 eq.), zinc nitrate hexahydrate $Zn(NO_3)_2{\cdot}6H_2O$ (0.060 g, 0.2 mmol, 1.5 eq.), urea (0.008 g, 0.13 mmol, 1 eq.) and distilled water (25 mL). The solution was stirred and heated at 140 °C and left at this temperature for 4 hours and cooled to room temperature. The final compound was obtained after filtration as a colorless powder, which was washed with distilled water, rinsed with ethanol and dried in air (quantity 19.2 mg; yield 64%).

Results and discussion

Diethyl 6-hydroxy-2-naphthylphosphonate (**1**) (precursor of the phosphonic acid **2**) was previously synthesized by using palladium(II) as the pre-catalyst and diethylphosphite as the reagent (Hirao's method).[55] With the aim of producing compound (**1**) in larger quantities (more than 10 g in one batch), we adapted the Tavs's method,[56] which uses Ni(II) as the pre-catalyst and triethylphosphite as the reagent (nickel assisted Arbuzov reaction).[57] For this reaction, we used $NiBr_2$ (Scheme 1) and employed 6-bromo-2-naphthol as the substrate directly without protecting the phenol function. During the synthesis, we observed the formation, in small quantities, of a side product resulting from the alkylation of the phenol function with an ethyl group. Then, we adapted the purification protocol to avoid purification by chromatography. First, compound (**1**) was purified by distillation (with a Kugelrohr distillation) at low pressure (5×10^{-2} mbar) and then the side product was discarded by liquid–liquid extraction. The expected compound (**1**) was isolated in 56% yield (14 g). Then, the phosphonate (**1**) was transformed into the phosphonic acid **2** by using the McKenna method.[57]

The phosphonic acid (**2**) was then used to prepare $M(H_2O)(O_3P\text{-}C_{10}H_6\text{-}OH)(H_2O)_{0.5}$ (with M = Mn^{2+}, Co^{2+}, Cu^{2+}, Zn^{2+}) by mixing it with either $Mn(NO_3)_2{\cdot}4H_2O$, $Co(NO_3)_2{\cdot}4H_2O$, $CuSO_4{\cdot}5H_2O$, or $Zn(NO_3)_2{\cdot}6H_2O$ in distilled water and in the presence of one equivalent of urea. Urea was used herein to slowly increase the pH of the reaction media during the hydrothermal treatment to favor the reaction of the phosphonic acid function with the metal salts as previously reported.[9] After hydrothermal treatment (120 to 140 °C for 24 hours), the crystals were recovered by filtration producing the materials (**3**)–(**6**) in yields ranging from 53% to 83%. The TGA analyses were then performed to determine the amount of water included in the structures and to assess the thermal stability of these materials (**3**)–(**6**). The TGA curves, recorded for the four compounds, show the same thermal decomposition behavior as a function of temperature (Fig. S1a†) and the main features are summarized in Table 1. As a representative example we selected $Mn(H_2O)(PO_3C_{10}H_6OH){\cdot}(H_2O)_{0.5}$ (**3**) (Fig. 1). From room temperature to 100 °C a first weight loss of 2.57% (calculated 2.96%) is observed. This result is in good agreement with the departure of the free half water molecule present in the formula. After this first dehydration step, a first plateau is observed from 100 °C to 150 °C, followed by a second weight loss of 5.82% (calculated 5.91%) between 150 °C and 200 °C associated with the departure of the coordination water molecule present in the inorganic layer. This second dehydration step leads to a second plateau observed from 200 °C to 341 °C. After this temperature, a final weight loss of 44.51% (calculated 46.66%) corresponding to the decomposition of the organic moiety and to the formation of the metal pyrophosphate $Mn_2P_2O_7$ at 1000 °C is observed. The final compound was clearly identified by powder X-ray diffraction and the total weight loss of 52.86% (calculated 53.19%) is in good agreement with the proposed formula.

Single crystal X-ray diffraction study

Single crystals were selected from batch numbers (**3**), (**4**), (**5**) and (**6**) and single crystal diffraction (XRSCD) experiments were performed as described in the ESI.† A monoclinic symmetry is observed for the different samples but with two different unit cells (see Table 2); the two fold axis characteristic of the monoclinic symmetry is running along the longer axis for the crystals from (**3**), (**4**) and (**6**) and along the shorter one

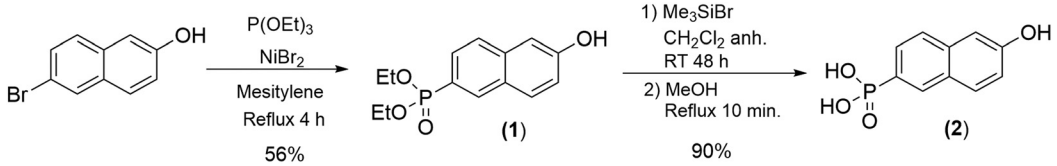

Scheme 1 Synthesis of 6-hydroxy-2-naphthylphosphonic acid (**2**) from 6-bromo-2-naphthol.

Table 1 Summary of the weight losses and dehydration temperatures obtained by thermogravimetric analysis under air at 2 °C min^{-1} for the four compounds $M(H_2O)(PO_3C_{10}H_6OH)\cdot(H_2O)_{0.5}$ (*found (calc.))

	$Mn(H_2O)(PO_3C_{10}H_6OH)\cdot(H_2O)_{0.5}$ (**3**)	$Co(H_2O)(PO_3C_{10}H_6OH)\cdot(H_2O)_{0.5}$ (**4**)	$Cu(H_2O)(PO_3C_{10}H_6OH)\cdot(H_2O)_{0.5}$ (**5**)	$Zn(H_2O)(PO_3C_{10}H_6OH)\cdot(H_2O)_{0.5}$ (**6**)
Weight loss ① (%)*	−2.57 (−2.96)	−2.89 (−2.92)	−2.3 (−2.87)	−2.65 (−2.86)
Temperature range (°C)	27 to 100	27 to 100	16 to 73	20 to 60
Temperature of the 1st plateau (°C)	100 to 150	100 to 150	73 to 124	60 to 73
Weight loss ② (%)*	−5.82 (−5.91)	−5.62 (−5.84)	−5.30 (−5.76)	−5.43 (−5.72)
Temperature range (°C)	150 to 200	150 to 195	124 to 157	73 to 98
Temperature of the 2nd plateau (°C)	200 to 341	195 to 350	157 to 279	98 to 335
Weight loss (**3**) (%)	−44.51 (−46.66)	−44.32 (−45.23)	−43.56 (−44.53)	−43.19 (−45.11)
Temperature range (°C)	341 to 1000	350 to 1000	279 to 1000	335 to 1000
Total weight loss (%)*	−52.90 (−55.53)	−52.83 (−53.74)	−51.16 (−53.54)	−51.27 (−53.48

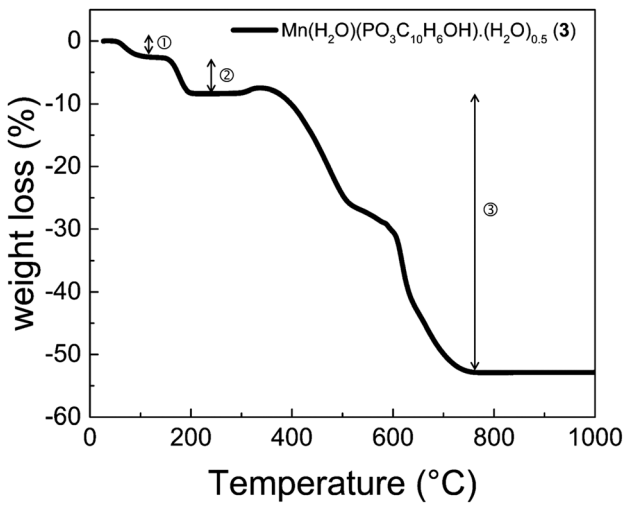

Fig. 1 Thermogravimetric curves of $Mn(H_2O)(PO_3C_{10}H_6OH)\cdot(H_2O)_{0.5}$ (**3**) recorded under air from room temperature to 1000 °C at the heating rate of 2 °C min^{-1}.

for the crystal from (**5**). Then, compounds (**3**), (**4**), (**6**), sharing the same unit cell, are considered as isostructural but a quite different structure is expected for (**5**). Moreover all the crystals tested from batch number (**6**) show a diffraction quality that is considered insufficient for structural analysis; only the unit cell obtained from XRSCD is presented in this study. On the basis of the unit cells summarized in Table 2, $Mn(H_2O)(PO_3C_{10}H_6OH)\cdot(H_2O)_{0.5}$ (**3**), $Co(H_2O)(PO_3C_{10}H_6OH)\cdot(H_2O)_{0.5}$ (**4**), $Zn(H_2O)(PO_3C_{10}H_6OH)\cdot(H_2O)_{0.5}$ (**6**) and $Cu(H_2O)(PO_3C_{10}H_6OH)\cdot(H_2O)_{0.5}$ (**5**) were analyzed using X-ray powder diffraction to check the homogeneity and the global quality of each synthesized batch. Le Bail[58] refinements confirmed the purity of all batches (Fig. ST2–ST5†). A structural analysis using single crystal data was then performed on the crystals of the (**3**), (**4**) and (**5**) batches; general information about the structural determination and refinement is given in the ESI.† The structural results obtained on the crystals of (**3**) and (**4**) are quite similar and confirm the assumption of isostructural materials. The cell parameters obtained for the crystal of (**6**), chemical analyses and a similar coordination expected for Zn^{2+} and Co^{2+} or Mn^{2+} lead to the hypothesis of a structure equivalent to compounds (**3**) and (**4**).

The main features are related to the lamellar characteristic of the structure: a regular stacking between one organic subnetwork and inorganic subnetwork along the *b* direction can be evidenced (Fig. 2). The inorganic subnetworks $[M(H_2O)PO_3C]$ present a perovskite-like structure made of corner sharing distorted $M^{2+}O_5\cdot H_2O$ octahedra connected *via* PO_3C tetrahedra from the organic building blocks 6-hydroxy-2-naphthylphosphonic acid (Fig. ST6†); each tetrahedron shares 3 O corners with 3 octahedra and one edge with a fourth one. Each octahedron is composed of one M^{2+} cation surrounded by five oxygen atoms belonging to the PO_3C group fully deprotonated and one oxygen atom emanating from one water molecule present in the apical position (dM^{2+}–$O(H_2O)$ ranging from 2.11 Å to 2.23 Å). The octahedra present a distortion depending on the nature of the metal transition cation and the distances between the oxygen of the PO_3C tetrahedron and the M^{2+} cation range from 2.116 Å to 2.355 Å. In the inorganic layer and depending on the nature of the cation M^{2+}, the distance between two phosphorus atoms of two PO_3C tetrahedra pointing in the same direction ranges from 5.660 Å to 7.467 Å along the *a* direction and 4.751 Å to 8.016 Å along the *c* direction (Table ST1†). The organic subnetwork is composed of the 6-hydroxynaphthyl moieties ($HO\text{-}C_{10}H_6$) organized in a double layer and is connected to the inorganic subnetwork by PO_3C tetrahedra. Within each layer, the 6-hydroxynaphthyl moieties present two different orientations: the black and the grey orientations drawn in Fig. 2; the black and grey moieties are oriented 31.6° apart. These two orientations are arranged as grey (GR) and black rows (BR) with a regular GR/BR/GR/BR stacking along the *a* direction (see Fig. 2). Consequently, this peculiar organization ensures two types of C···H–C hydrogen bonds between two neighboring rings ranging from 3.080 Å to 3.294 Å (Fig. ST6 and Table ST2†). Additionally, within two inorganic layers the naphthalene rings form pairs of ligands connected together through the hydroxyl function and the free water molecule. Thus, between two adjacent organic layers, these pairs of ligands are organized in a zig–zag pattern along the *b* direction for compounds $Mn(H_2O)(PO_3C_{10}H_6OH)\cdot(H_2O)_{0.5}$ (**3**), $Co(H_2O)(PO_3C_{10}H_6OH)\cdot(H_2O)_{0.5}$ (**4**) and $Zn(H_2O)(PO_3C_{10}H_6OH)\cdot(H_2O)_{0.5}$ (**6**). The large distances between the aromatic rings, which are imposed by the distances between the phosphorus atoms and the tilt angle of

Table 2 Single crystal X-ray diffraction data of $Mn(H_2O)(PO_3C_{10}H_6OH)\cdot(H_2O)_{0.5}$ (**3**), $Co(H_2O)(PO_3C_{10}H_6OH)\cdot(H_2O)_{0.5}$ (**4**), $Cu(H_2O)(PO_3C_{10}H_6OH)\cdot(H_2O)_{0.5}$ (**5**) and $Zn(H_2O)(PO_3C_{10}H_6OH)\cdot(H_2O)_{0.5}$ (**6**)

Formula	$Mn(H_2O)(PO_3C_{10}H_6OH)\cdot(H_2O)_{0.5}$ (**3**)	$Co(H_2O)(PO_3C_{10}H_6OH)\cdot(H_2O)_{0.5}$ (**4**)	$Cu(H_2O)(PO_3C_{10}H_6OH)\cdot(H_2O)_{0.5}$ (**5**)	$Zn(H_2O)(PO_3C_{10}H_6OH)\cdot(H_2O)_{0.5}$ (**6**)
Molecular formula	$MnC_{10}PO_{5.5}H_{10}$	$CoC_{10}PO_{5.5}H_{10}$	$CuC_{10}PO_{5.5}H_{10}$	$ZnC_{10}PO_{5.5}H_{10}$
FW (g mol^{-1})	304.1	308.08	312.70	314.54
SG	$P12_1/c1$	$P12_1/c1$	$P12_1/n1$	$P12_1/c1$
a (Å)	7.4672(3)	7.3353 (3)	5.66017 (4)	7.290(5)
b (Å)	40.7737 (9)	40.691 (2)	4.75153 (4)	40.86(3)
c (Å)	7.6132(10)	7.4400 (2)	41.0950 (3)	7.547(5)
α (°)	90	90	90	90
β (°)	99.045(8)	99.144 (4)	93.0499 (6)	99.48(8)
γ (°)	90	90	90	90
z	4	4	4	4
V (Å^3)	2289.1 (3)	2192.50(4)	1103.662(3)	2217.3(5)
d_{calc} (g cm^{-3})	1.759	1.867	1.867	
μ mm^{-1}	1.303	1.722	5.416	
Radiation source λ (Å)	Mo Kα 0.71073	Mo Kα 0.71073	Cu Kα 1.54184	
Pattern range 2θ (°)	5.5–79.06	5.63–68.27	8.620–151.744	
No. of reflections	12 166	7693	26 244	
No. of soft constrains	0	0	0	
Weighted R factor	0.1256	0.1137	0.0958	
$R[F^2 > 2\sigma(F^2)]$	0.1031	0.0992	0.0958	
R_{int} (internal R value)	0.1311	0.0280	0.0286	
S (goodness of the fit)	2.40	1.055	1.289	

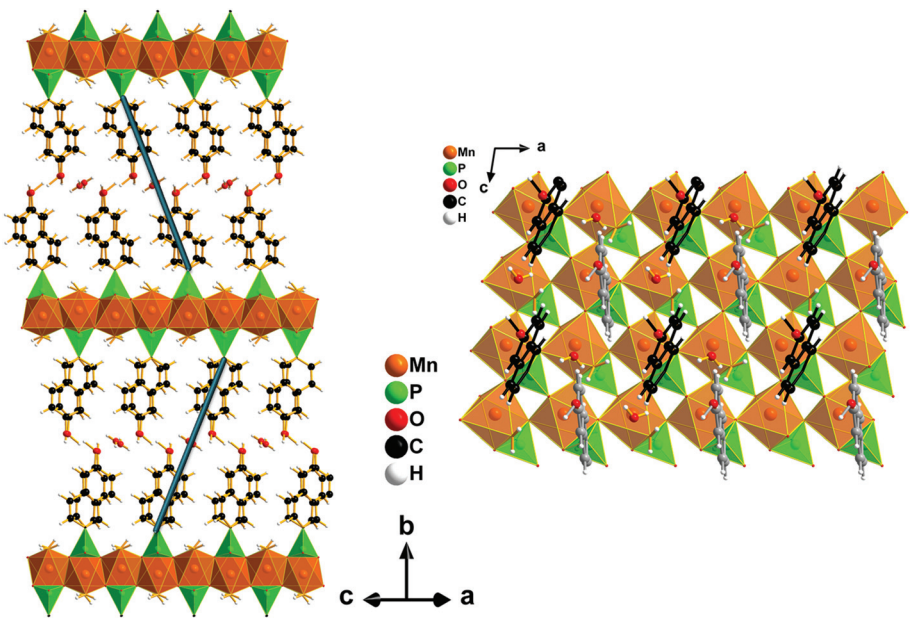

Fig. 2 View of the organic–inorganic lamellar structure of the compound $Mn(H_2O)(PO_3C_{10}H_6OH)\cdot(H_2O)_{0.5}$ (**3**); the blue line indicates the zig–zag organization of the organic pairs.

31.6° between them, do not allow strong π···π stacking. This result contrasts with a previous example featuring unsubstituted naphthyl based metallophosphonates[39] that feature π···π stacking and that likely explain the enhanced luminescence properties. Finally, cohesion of the structure is ensured by a hydrogen bond O–H···O network, with distances ranging from 1.6 Å to 3.4 Å, due to the presence of the phenol functions and the free water molecules at the interface of two organic layers. This network of hydrogen bonds is composed of two different types of O–H···O interaction involving either two phenol functions from two organic layers or one free water molecule and one-phenol function, both of which contribute to the cohesion of the structure (Fig. ST7 and Table ST5†). The structure of compound (**5**) is described hereafter. The observed unit cell shows differences with the one evidenced for Co, Mn and Zn based materials but the main characteristics of the previous samples can be found for $Cu(H_2O)(PO_3C_{10}H_6OH)\cdot(H_2O)_{0.5}$ such as the existence of an inorganic and one inorganic sub

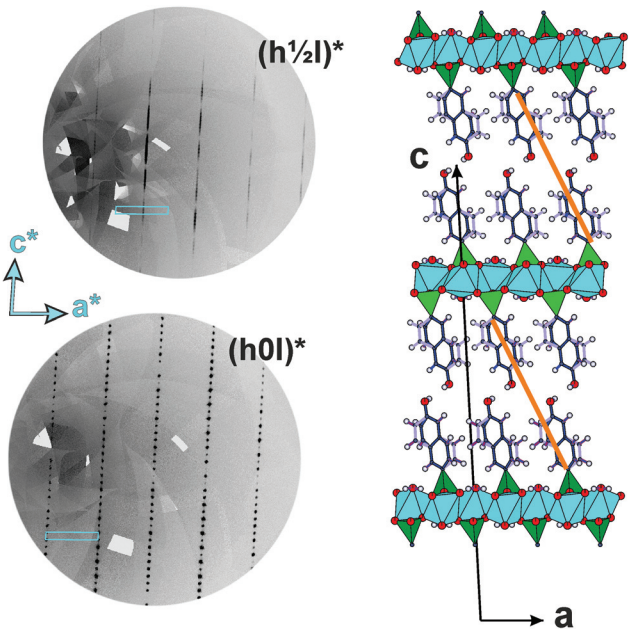

Fig. 3 Representation of the plan (h $\frac{1}{2}$ l)*and (h 0 l)* plan showing the diffuse scattering running along the c* direction and view of the organic–inorganic lamellar structure of the compound $Cu(H_2O)(PO_3C_{10}H_6OH)\cdot(H_2O)_{0.5}$ (**5**); the orange line represents the parallel organization of organic pairs.

network periodically but stacked along the c direction (Fig. 3). However, the structural analysis reveals disorder phenomena at the level of the organic slab. A direct manifestation of this disorder is the splitting of 4 carbon atoms on two positions with an occupancy of 50% as shown in Fig. 4a. A possible interpretation of such a feature is the existence of two possible orientations for the 6-hydroxy-2-naphthylphosphonic groups. These two orientations can be evidenced in Fig. 4b; an angle of about 32° between these two equiprobable orientations

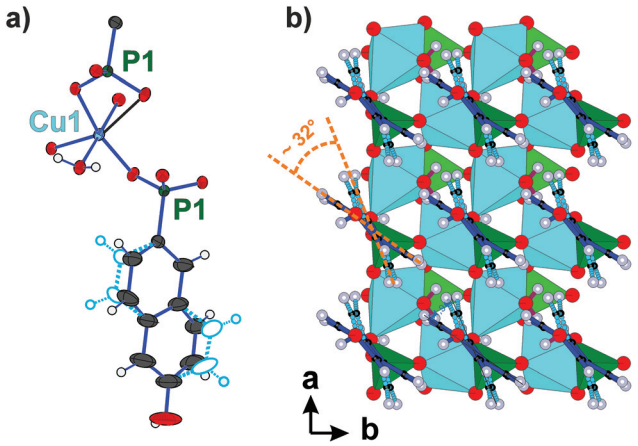

Fig. 4 (a) Representation of the two possible organizations in $Cu(H_2O)(PO_3C_{10}H_6OH)\cdot(H_2O)_{0.5}$, (b) showing in orange the dashed line at the angle of 32° between the two organic possibilities.

must be discussed in the light of the organization of the 6-hydroxy-2-naphthylphosphonic groups evidenced for Mn $(H_2O)(PO_3C_{10}H_6OH)\cdot(H_2O)_{0.5}$. In the Mn based sample, as shown in Fig. 2, the neighboring rings are tilted with a very similar angle of 31.6° along the stacking direction. Furthermore, consider the (h 0 l)* and (h $\frac{1}{2}$ l)* diffraction plans drawn in Fig. 4. Diffuse scattering lines running along c* are observed at the $\frac{1}{2}a^* + \frac{1}{2}b^*$ position. This diffraction feature is in agreement with a structural ordering leading to a doubling of the periodicity along a and b but with a loss of correlation along the stacking direction. Considering this observation, the existence of equiprobable orientations of 6-hydroxy-2-naphthylphosphonic groups and the perfect ordering evidenced for Mn $(H_2O)(PO_3C_{10}H_6OH)\cdot(H_2O)_{0.5}$, the disorder in $Cu(H_2O)(PO_3C_{10}H_6OH)\cdot(H_2O)_{0.5}$ can be interpreted on the basis of perfectly ordered organic $(PO_3C_{10}H_6OH)$ plans built up with a perfect ordering of the two orientations of the 6-hydroxy-2-naphthylphosphonic acid (as reported for the structure of Mn based compound with GR and BR) but with a possible loss of ordering from plan to plan in the stacking direction.

A comparison of the projections along [101] for the Mn based compound (Fig. 2) and along [010] for the Cu based compound (Fig. 4) shows the same structural orientation. The observation along the stacking direction of two adjacent double $(PO_3C_{10}H_6OH)$ layers pointed out an interesting difference between the two samples. The zig–zag pattern observed for the pairs of ligands running along the b direction for compounds (**3**), (**4**) and (**6**) is replaced with a parallel orientation (orange segment in Fig. 3).

On the basis of the thermogravimetric analysis, the study of the evolution of the cell parameters as a function of the amount of water molecules present in the structure of the compound $Mn(H_2O)(PO_3C_{10}H_6OH)\cdot(H_2O)_{0.5}$ (**3**) chosen as the representative element of the whole series, was conducted by X-ray powder diffraction as a function of temperature. For this purpose, powder X-ray diffraction patterns were recorded at 30 °C, 65 °C, 100 °C, 120 °C, 150 °C and 220 °C which correspond to temperatures taken on the plateaus of the thermogravimetric curve associated to the dehydration process ① and ② of the compound (see Fig. 1 and Fig. S1b†).

To follow the evolution of the cell parameters of $Mn(H_2O)(PO_3C_{10}H_6OH)\cdot(H_2O)_{0.5}$ at each of these temperatures (Fig. 5), the X-ray diffraction patterns were automatically indexed by using the DICVOL[59] software from the FULLPROF[60] program suite. The diffraction pattern recorded at 30 °C was used to validate our methodology and was first automatically indexed in a monoclinic cell with the parameters a = 5.756 Å, b = 40.979 Å, c = 4.913 Å, β = 90.96°, and V_{cell} = 1158 Å^3 which amounted to half of the monoclinic cell obtained on a single crystal. This second cell was then deduced from the first cell by the use of the appropriate transformation matrix (see the ESI Fig. ST6†) leading to the following parameters a = 7.505 Å, b = 40.979 Å, c = 7.630 Å, β = 99.1°, and V_{cell} = 2366 Å^3 which were found to be in agreement with those of the single crystal (a = 7.467 Å, b = 40.774 Å, c = 7.613 Å, β = 99.045°, V_{cell} = 2289.1 Å^3). This result demonstrated that up to 150 °C the a

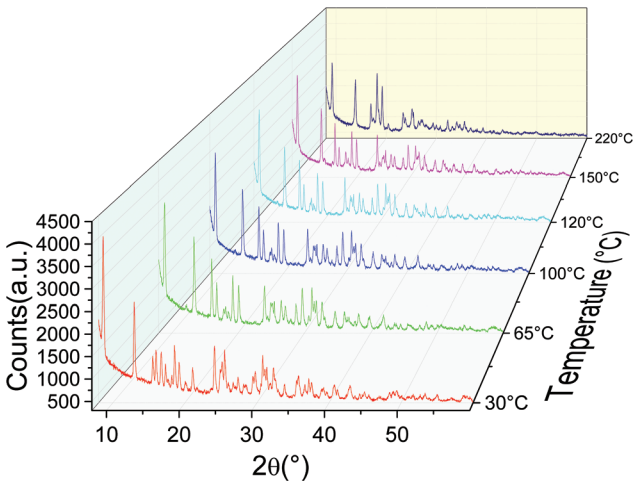

Fig. 5 Powder X-ray diffraction patterns of $Mn(H_2O)(PO_3C_{10}H_6OH)\cdot(H_2O)_{0.5}$ (**3**) recorded at 30 °C, 65 °C, 100 °C, 120 °C, 150 °C and 220 °C.

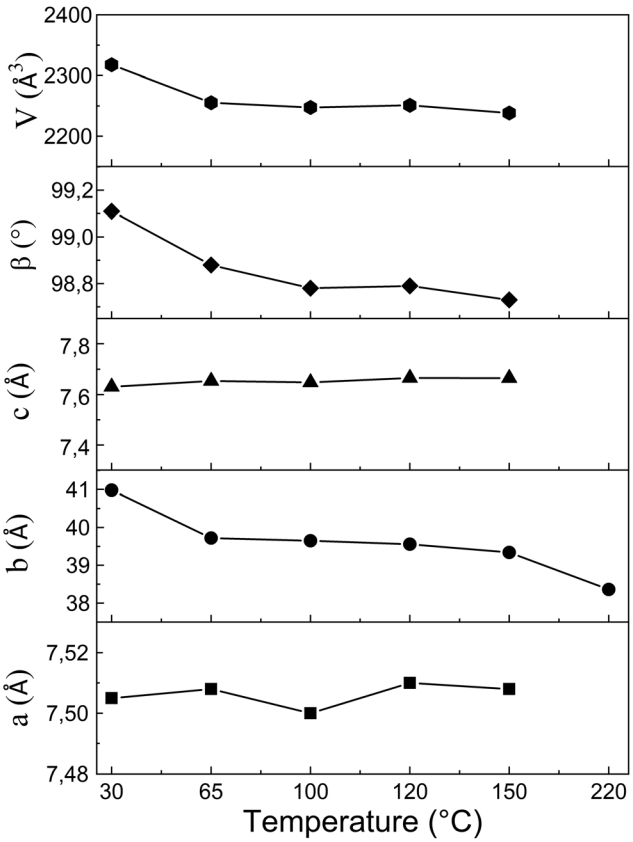

Fig. 6 Variation of the cell parameters of $Mn(H_2O)(PO_3C_{10}H_6OH)\cdot(H_2O)_{0.5}$ (**3**) calculated by using the DICVOL software from 30 °C to 220 °C.

and *c* parameters of the monoclinic cell remained constant and the *b* parameter showed a significant decrease in the function of temperature (Fig. 8). At 220 °C, the PXRD pattern is strongly modified, which is indicative of a structural transition associated with the departure of the water molecule bonded to the Mn. The DICVOL software gives several indexing results and it is not possible to identify the actual cell parameters. Nevertheless, the *b* axis, easily identifiable, is always equal to 38.4 Å. The variation of this cell parameter corroborates the results obtained by thermogravimetric analyses. Indeed from 65 °C to 150 °C, the departure of the half water molecule present at the interface of two organic layers can be associated with the decrease of the interlamellar distance (40.97 Å to 39.35 Å) and thus with the contraction of the volume of the monoclinic cell. This decrease occurs without any structural modification of the inorganic subnetwork $[Mn(H_2O)PO_3C]$ as shown by the constancy of the in plane parameters *a* and *c*. After 220 °C, the departure of the water molecule present around the $MnO_5\cdot H_2O$ octahedron is associated with the significant structural changes of the inorganic subnetwork as shown by the drastic change of the *b* cell parameter related to a new contraction of the interlamellar distance and cell volume. This X-ray diffraction study performed from room temperature to 220 °C allowed us to confirm that the compound $Mn(H_2O)(PO_3C_{10}H_6OH)\cdot(H_2O)_{0.5}$ preserved a lamellar structure during its dehydration process, which is associated with a contraction of its interlayer distances (Fig. 6).

Magnetic properties

The magnetic properties of compound (**3**) are presented in Fig. 7. The fit of the $1/\chi = f(T)$ curve in the high temperature region (above 200 K) leads to a Curie constant of 3.81 emu K mol^{-1}, which is smaller than the expected value of 4.375 emu K mol^{-1} for $S = 5/2$ ion considering $g = 2$, and a negative Weiss temperature of −24 K, which indicates dominant antiferromagnetic interactions. At low temperatures, $\chi = f(T)$ presents a broad hump centered at 20 K, corresponding to 2D antiferromagnetic short range interactions.[38,61]

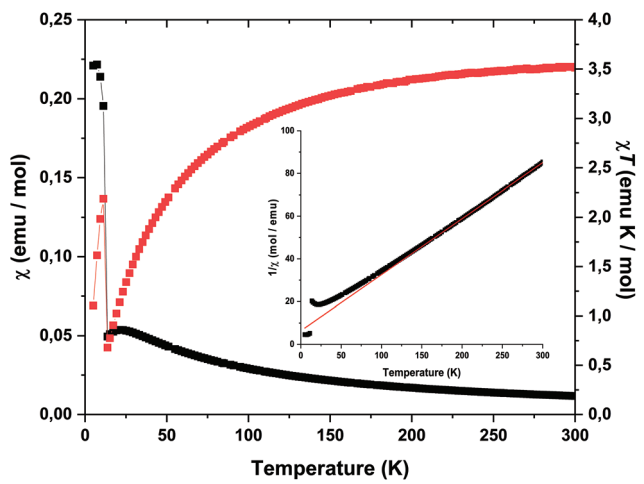

Fig. 7 χ (black squares) and χT (red squares) as a function of temperature under a dc field of 100 Oe (zfc mode) for compound (**3**) (the thin lines are just a guide for the eye). The thick red line corresponds to the best fit, see text. Inset: $1/\chi = f(T)$; the Curie–Weiss law fit for $T > 200$ K is indicated in red.

The $\chi = f(T)$ curve was fitted with a 2D high temperature series expansion for a square planar layer of Heisenberg spins $S = 5/2$ for T above 15 K (below this temperature, 3D correlations invalidate the model).[62] The fit leads to $J = -1.9$ cm^{-1} (considering a Hamiltonian in the form $\mathcal{H} = -J\sum_{ij} S_i \cdot S_j$), in the same range as the exchange interactions reported for similar systems.[61]

When the temperature decreases further, $\chi = f(T)$ shows a sharp increase at 12 K, and the zfc and fc curves start diverging (Fig. 8a). This indicates the occurrence of magnetic transition, corresponding to a 3D ordering. In order to make an in-depth study of this behavior, we performed ac susceptibility measurements at 1 Hz and 11 Hz (Fig. 8c). At 20 K, the broad hump centered at 20 K is observed in χ' but not in χ'', as expected for 2D antiferromagnetic behavior. At 12.2 K, both χ' and χ'' present a sharp peak, the position of which does not depend on the frequency of the oscillating field. Interestingly, this feature disappears upon the application of a dc field larger than 3 T Fig. 8b. This overall behavior can be ascribed to a canted antiferromagnetic ordering below 12.2 K as has been previously described for other Mn phosphonate layered compounds.[38,61,63–65]

The M *vs.* H curve (Fig. 9) does not show opening of a hysteresis, as expected for canted antiferromagnets with a very small canting angle.[64,66] The spin–flop transition is evidenced for $T < T_N$ by the sigmoidal shape at around 2.5 T. This spin flop disappears when the temperature increases above T_N.

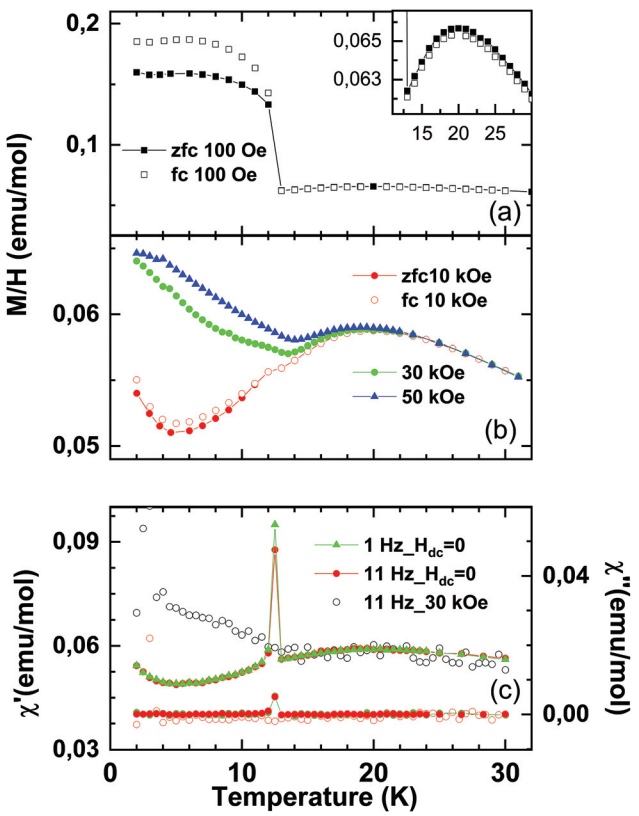

Fig. 8 zfc and fc curves for compound (**3**) under an applied dc field of 100 Oe (a), 10 kOe and 30 kOe (b). ac susceptibility curves (1 Oe oscillating field) at various frequencies and an applied dc field (c).

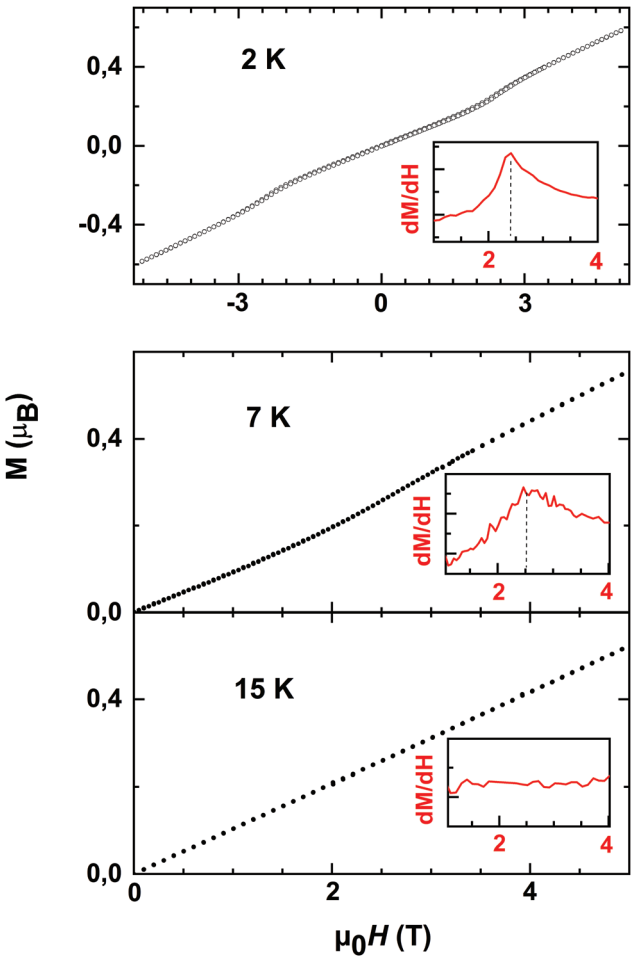

Fig. 9 Magnetization *vs.* field curves at various temperatures for compound (**3**). Insets: corresponding derivative curves.

The cobalt analogue (**4**) displays antiferromagnetic behavior as evidenced by the broad maximum in the $\chi = f(T)$ curve, characteristic of 2D antiferromagnetic interactions (Fig. 10). Such behavior is identical to the one previously described for $Co(O_3PC_6H_5)\cdot H_2O$.[61,66] The fit of the $1/\chi = f(T)$ curve in the high temperature region (above 150 K) leads to a Curie constant of 3.87 emu K mol^{-1}, which is in agreement with the expected value for HS Co(II) ions in octahedral sites[67] and a negative Weiss temperature of −60 K. The 2D magnetic behavior is fitted in the high temperature region ($T > 40$ K) using the high temperature series expansion for a square planar layer of Ising spins $S = 1/2$.[68] The fit leads to $J = -6.9$ cm^{-1}. Contrary to what is observed in the case of another layered cobalt phosphonate, $Co_3(O_3PC_2H_4CO_2)_2$, made with a phosphonate/carboxylate ligand, for which both carboxylate and phosphonate groups are coordinated, leading to corrugated inorganic layers and different magnetic exchange pathways, no canted antiferromagnetic order is observed here.[69]

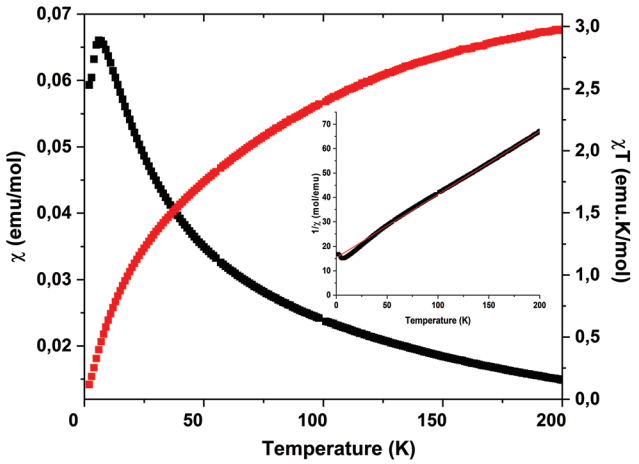

Fig. 10 χ (black squares) and χT (red squares) as a function of temperature under a dc field of 100 Oe (zfc mode) for compound (**4**). The thick red line corresponds to the best fit (see text). Inset: $1/\chi = f(T)$; the Curie–Weiss law fit for $T > 150$ K is indicated in red.

Finally, the copper analogue (**5**), presents a different magnetic behavior. The fit of the $1/\chi = f(T)$ curve in the high temperature region (above 200 K) leads to a Curie constant of 0.386 emu K mol^{-1}, which is in good agreement with the expected value 0.375 emu K mol^{-1} for $S = 1/2$ ion considering $g = 2$, and a positive Weiss temperature of 31 K, which underlines the occurrence of dominant ferromagnetic interactions (Fig. 11).

The rapid increase of χ and χT at low temperature when the temperature decreases suggests the occurrence of a 3D ferromagnetic ordering at a low temperature (around 2 K). A full understanding of the origin of these ferromagnetic interactions and of the ferromagnetic ordering is beyond the scope of the present work. Yet, it is worth underlining that such ferromagnetic interactions in layered phosphonates with a perovskite-like structure are rare[70] and to the best of our knowledge it is the first time they are observed for a copper-based compound.

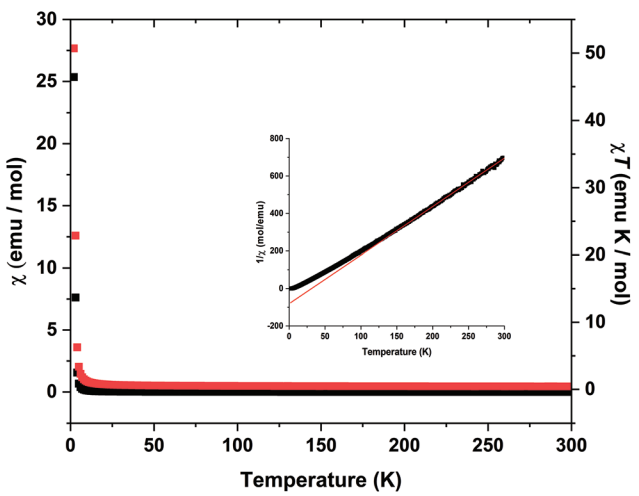

Fig. 11 χ (black squares) and χT (red squares) as a function of temperature under a dc field of 100 Oe (zfc mode) for compound (**4**). Inset: $1/\chi = f(T)$; the Curie–Weiss law fit for $T > 200$ K is indicated in red.

Luminescence properties

The UV/Vis absorbance spectra of the ligand and four compounds (Fig. 12) show absorption bands ranging from deep UV to visible. The absorbance spectra from ligand (**2**) and compounds were subtracted from the baseline and were fitted by the number of observed bands by means of Voigt functions. At shorter wavelengths several strong absorption bands were observed for ligand (**2**) and compounds (**3**)–(**6**). The ligand showed absorption bands at 237 nm, 299 nm and 336 nm. Mn^{2+} compounds (**3**) showed absorption bands at 215 nm and 302 nm. Co^{2+} compounds showed absorption bands at 240 nm and 300 nm. Cu^{2+} compounds showed absorption bands at 216 nm and 272 nm. Zn^{2+} compounds showed absorption bands at 225 nm and 295 nm. The similarity of the most intense absorbance bands located at shorter wavelengths for the ligand and compounds testifies to the fact that the main mechanism of optical absorption is governed by a common based moiety.[71–74] Those first bands are associated with the singlet transitions S0 → S1 (290–320 nm), S0 → S2 (240–290 nm), or S0 → S3 (200–230 nm) of the naphthalene moieties present in ligand (**2**) and compounds (**3**)–(**6**) and which are observed in solution or in solid form.[74] At larger wavelengths, absorption bands appear to be located at different positions depending on the nature of the compounds. Ligand (**2**) shows a supplementary band located at 482 nm. Compound (**3**) shows supplementary absorption bands at 423 nm. The compound with Co^{2+} shows absorption bands at 434 nm and a supplementary band at 539 nm is attributed to the Co^{2+} transition $^4T_{1g}(F) \rightarrow {}^4A_{2g}(F)$ or $^4T_{1g}(F) \rightarrow {}^4T_{1g}(P)$.[76] Compound (**5**) shows supplementary absorption bands: one at 425 nm and one at 849 nm. The latter is attributed to the $^2E_g \rightarrow {}^2T_{2g}$ transition.[77] Compound (**6**) shows a supplementary absorption band at 432 nm. The origin of the bands located at 482, 423, 434, 425 and 432 nm for ligand (**2**) and Mn^{2+} (**3**), Co^{2+} (**4**), Cu^{2+} (**5**) and Zn^{2+} (**6**) respectively remains not fully explained. However, the similarity in those bands in the ligand and compounds may indicate a common origin. For Mn^{2+} and Co^{2+} compounds it could be partially attributed to the $^6A_1(S) \rightarrow {}^4T_{1g}(G)$, $^4T_{2g}(G)$, $^4A_{1g}(G)$, and $^4T_{2g}(D)$ transitions and to the $^4T_{1g}(F) \rightarrow {}^2T_{1g}(P)$ and $^4A_{1g}(G)$–$^4T_{1g}(P)$ transitions respectively.[73,74]

The photoluminescence spectra of ligand (**2**) and the four compounds (**3**)–(**6**) excited at 266 nm are shown in Fig. 13. The emission spectra from ligand (**2**) and the hybrid materials were subtracted from the instrumental baseline and were fitted by the number of observed bands by means of Voigt functions (Table 3). The PL spectra presented in Fig. 13 show a comparable intensity for ligand (**2**) and Zn compounds (**6**), while the Mn compound (**3**) and Co compound (**4**) show a PL intensity ten and one hundred times lower than that for ligand (**2**), respectively. Cu compound (**5**) does not show any emission

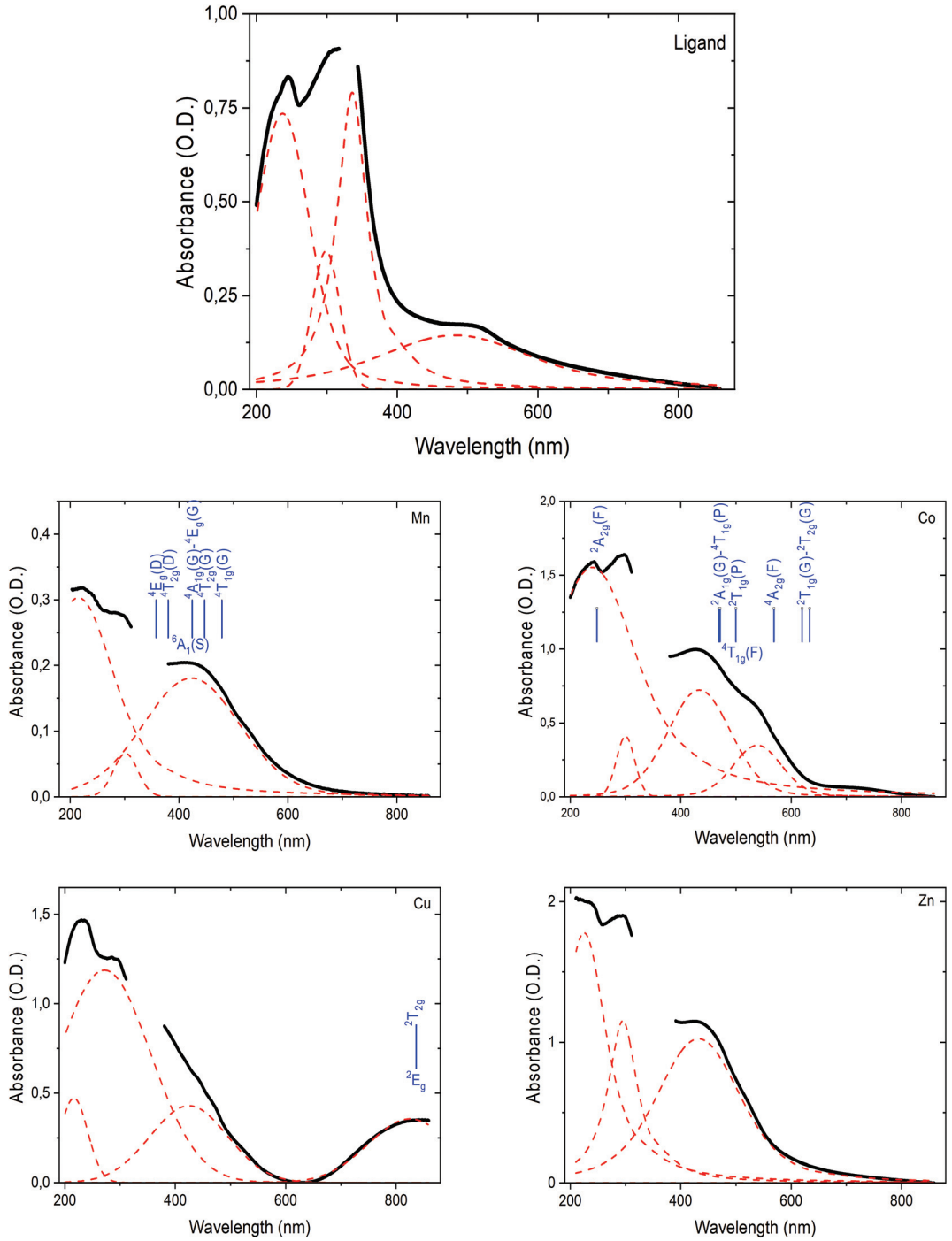

Fig. 12 Absorbance spectra fitted by Voigt functions of ligand (**2**) and Mn^{2+} (**3**), Co^{2+} (**4**), Cu^{2+} (**5**) and Zn^{2+} (**6**) compounds with an absorption band of transition metal in II oxidation state and in octahedral symmetry reported for Mn^{2+} (**3**),[75] for Co^{2+} (**4**),[76] and for Cu^{2+} (**5**).[77]

bands. The ligand (**2**) spectrum shows two intense emission peaks located at 362 (P1) and 408 nm (P2) and a weaker peak located at 486 nm (P3). The four compounds show different emission behaviors that are presented hereafter. Compound (**3**) shows four weak emission bands located at 362 nm, 424 nm, 517 nm and 649 nm. Compound (**4**) shows one weak emission band located at 360 nm, and a broad peak at 542 nm. Finally, compound (**6**) shows three emission bands located at 363 nm, 420 nm, and 537 nm. Except for the Cu^{2+} based hybrid, the three other compounds show a first PL peak at a similar position than the P1 peak observed with ligand (**2**). The band at 649 nm for hybrid (**3**) can be assigned to the spin forbidden $^4T_{1g}(G) \rightarrow {}^6A_{1g}(S)$ transition of Mn^{2+} ion in the octahedral symmetry site.[78,79] The presence of Cu^{2+} completely

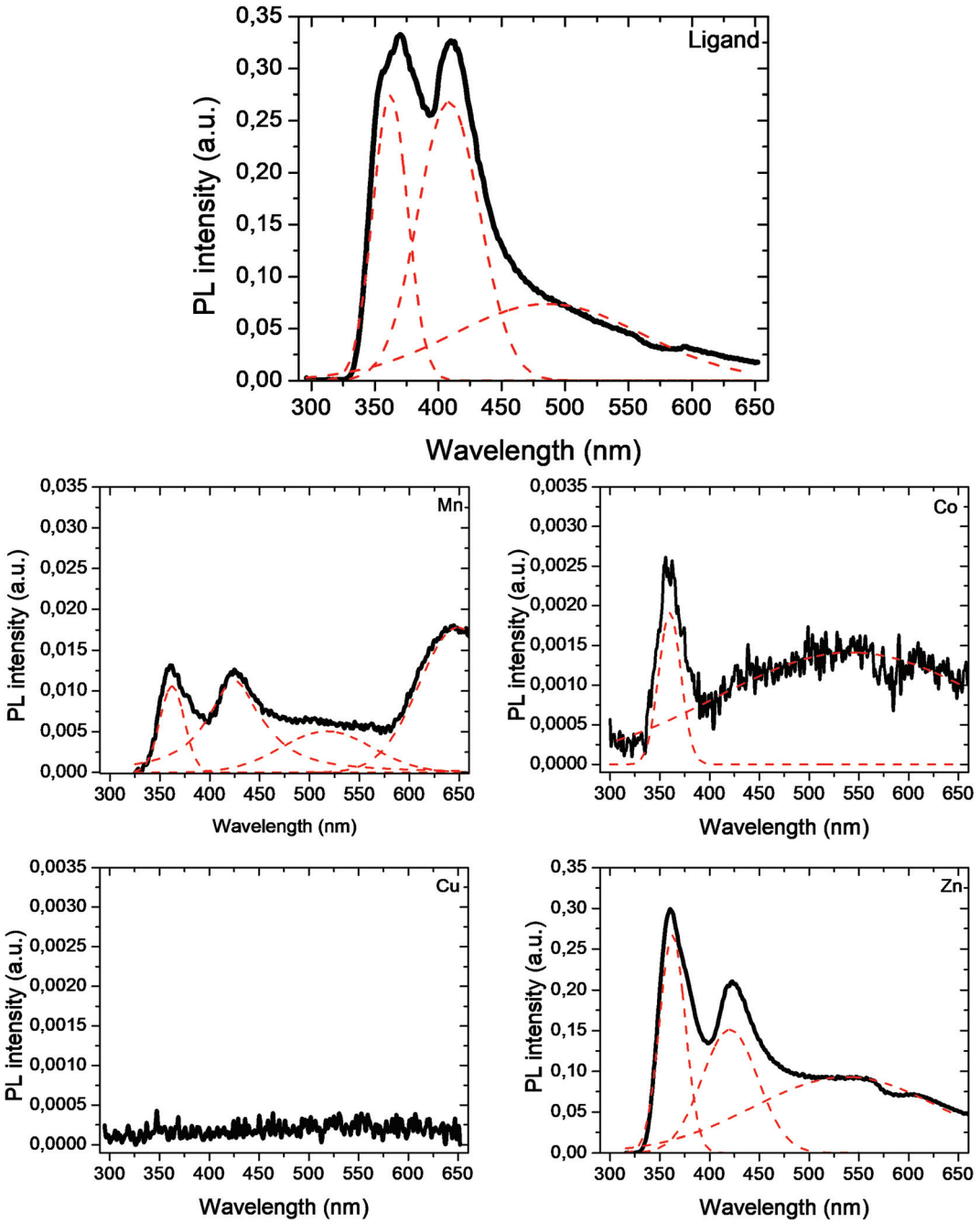

Fig. 13 Photoluminescence spectra of ligand **2**, Mn^{2+} (**3**), Co^{2+} (**4**), Cu^{2+} (**5**) and Zn^{2+} (**6**) compounds and emission bands fitted by means of Voigt functions.

Table 3 Tabulated luminescence bands for the ligand and the four compounds $M(H_2O)(PO_3C_{10}H_6OH)\cdot(H_2O)_{0.5}$

Bands (nm)	2-Naphthylphosphonic acid (**2**)	$Mn(H_2O)(PO_3C_{10}H_6OH)\cdot(H_2O)_{0.5}$ (**3**)	$Co(H_2O)(PO_3C_{10}H_6OH)\cdot(H_2O)_{0.5}$ (**4**)	$Cu(H_2O)(PO_3C_{10}H_6OH)\cdot(H_2O)_{0.5}$ (**5**)	$Zn(H_2O)(PO_3C_{10}H_6OH)\cdot(H_2O)_{0.5}$ (**6**)
1	362 (P1)	362	360		363
2	408 (P2)	424	542		420
3	486 (P3)	517			537
4		649			

quenches the emission as previously evidenced for Cu^{2+} complexes featuring fluorophore moieties[80] and in copper–fluorenephosphonate.[26] This might be due to photoinduced electron-transfer mechanisms resulting in a PL quenching.[81] Zn compound (**6**) shows three bands that cannot be attributed to the presence of Zn^{2+} and considering its full $3d^{10}$ electronic configuration no electron can be promoted to a higher level by an excitation process with energy up to the visible level. This is in agreement with the fact that Zn^{2+} alone does not present any absorption bands. The naphthalene moieties present in ligand (**2**) and hybrids (**3**)–(**6**) exhibit singlet–singlet radiative recombination from 310 to 390 nm, and under some conditions of the saturated solution, show excimer-type emission ranging from 375 to 420 nm.[22] Thus, emission bands in the range of 310 to 420 nm may be attributed to singlet–singlet recombination and to possible excimer like emission[22] originating from the naphthalene moiety in the ligand and hybrids. The band at 542 nm for Co compound (**4**) could be attributed to recombination occurring from the level $^2T_{1g}(H)$ to the ground level $^4T_{1g}(F)$ in the octahedral symmetry site.[82] However, this band is close to similar bands observed with compounds (**3**) and (**6**) at 517 and 537 nm respectively and considering the slight redshift that is relatively similar to band P3 (486 nm) observed with the ligand. This may indicate a common origin of those bands, which could be attributable to the common naphthalene moiety into the ligand and hybrids. This kind of red shifted emission has been observed in a previous paper[22] on ligands and hybrids however, the structure of those compounds (**2**), (**3**), (**4**), (**6**) does not allow us to conclude straightforwardly the same origin of this red shifted emission. *Ab initio* based investigations of the electronic configurations of ligands and compounds are required to further explain the origin of those emission bands.

Conclusion

In this study we present the synthesis, structural characterization, magnetic and luminescence properties of four metallophosphonate $M(H_2O)(PO_3C_{10}H_6OH)\cdot(H_2O)_{0.5}$ (M = Mn, Co, Cu, Zn) obtained by hydrothermal synthesis from 6-hydroxy-2-naphthylphosphonic acid. These materials present a similar structural architecture made of perovskite-like inorganic layers alternating with 6-hydroxy-2-naphthyl moieties stacked in a double layer within the organic network. Moreover, despite the similar architecture of the inorganic network of these compounds, the X-ray diffraction study performed on single crystals has allowed us to evidence that in the Mn, Co compounds the organic pairs of the 6-hydroxy-2-naphthyl moieties present a zig–zag organization whereas in the Cu compound these pairs are organized in parallel. A structural study conducted by X-ray diffraction on powder samples on the Mn compound allowed us to follow the variation of the interlayer parameter as a function of temperature. The study of the magnetic properties of these materials reveals an overall antiferromagnetic behavior for the Co and Mn analogues, with the occurrence of a canted antiferromagnetic order at T_N = 12.2 K for the Mn analogue and a ferromagnetic behavior for the copper analogue, which will be studied more thoroughly in a subsequent work. Finally, the luminescence study has revealed common absorption emission properties at short wavelengths attributed to singlet–singlet and excimer like transitions originating from the common naphthalene based moieties in ligand (**2**) and hybrids (**3**), (**4**), (**5**) and (**6**). The compounds with the transition metals Mn^{2+}, Co^{2+}, and Cu^{2+} have shown different absorption and emission properties indicating the contribution of transition metals to those optical properties. The ligand and compounds with Mn^{2+}, Co^{2+}, Zn^{2+} present a red shifted emission, which is relatively similar to the one observed in our previous work,[22] and which remains unexplained yet and will therefore need further investigations.

Conflicts of interest

There are no conflicts to declare.

Acknowledgements

The authors thank the Agence Nationale de la Recherche [contract No. ANR-14-CE07-0004-01 (HYMN)] for financial support. We thank the platforms (RMN-RPE and spectrométrie de masse) from the University of Brest.

References

1 A. Clearfield and J. A. Stynes, *J. Inorg. Nucl. Chem.*, 1964, **26**, 117–129.
2 G. Alberti, U. Costantino, S. Alluli and N. B. Tomassini, *J. Inorg. Nucl. Chem.*, 1978, **40**, 1113–1117.
3 C. Y. Yang and A. Clearfield, *React. Polym., Ion Exch., Sorbents*, 1987, **5**, 13–21.
4 A. Clearfield and K. Demadis, *Metal Phosphonate Chemistry: From synthesis to application*, RSC Publishing, 2011. ISBN: 978-1-84973-356-4.
5 A. Clearfield, *Chem. Rev.*, 1988, **88**, 125–148.
6 A. Clearfield, *Inorganic Ion Exchange Materials*, CRC Press, 2018, ISBN: 978-1-315-89446-1.
7 R. Silbernagel, C. H. Martin and A. Clearfield, *Inorg. Chem.*, 2016, **55**, 1651–1656.
8 N. Stock and T. Bein, *Angew. Chem., Int. Ed.*, 2004, **43**, 749–752.
9 (*a*) J. M. Rueff, V. Caignaert, S. Chausson, A. Leclaire, C. Simon, O. Perez, L. le Pluart and P. A. Jaffrès, *Eur. J. Inorg. Chem.*, 2008, 4117–4125; (*b*) J. M. Rueff, M. Poienar, A. Guesdon, C. Martin, A. Maignan and P. A. Jaffrès, *J. Solid State Chem.*, 2016, **236**, 236–245.
10 S. Konar and A. Clearfield, *Inorg. Chem.*, 2008, **47**, 3489–3491.
11 Z. Chen, Y. Zhou, L. Weng, C. Yuan and D. Zhao, *Chem. – Asian J.*, 2007, **2**, 1549–1554.

12 P. J. Byrne, D. S. Wragg, J. E. Warren and R. E. Morris, *Dalton Trans.*, 2009, 795–799.
13 M. Wilke, A. Kabelitz, A. Zimathies, K. Radema and F. Emmerling, *J. Mater. Sci.*, 2017, **52**, 12013–12020.
14 K. J. Gagnon, H. P. Perry and A. Clearfield, *Chem. Rev.*, 2012, **112**, 1034–1054.
15 P. A. Jaffrès, V. Caignaert and D. Villemin, *Chem. Commun.*, 1999, 1997–1998.
16 J. M. Taylor, R. Vaidhyanathan, S. S. Iremonger and G. K. H. Shimizu, *J. Am. Chem. Soc.*, 2012, **134**, 14338–14340.
17 S. J. I. Shearan, N. Stock, F. Emmerling, J. Demel, P. A. Wright, K. D. Demadis, M. Vassaki, F. Costantino, R. Vivani, S. Sallard, I. R. Salcedo, A. Cabeza and M. Taddei, *Crystals*, 2019, **9**, 270.
18 G. Maheut, M. Hervieu, C. Fernandez, V. Montouillout, D. Villemin and P. A. Jaffrès, *J. Mol. Struct.*, 2003, **659**, 135–142.
19 C. Maillet, P. Janvier, M. Pipelier, T. Praveen, Y. Andres and B. Bujoli, *Chem. Mater.*, 2001, **13**, 2879–2884.
20 T. Sawano, N. C. Thacker, Z. Lin, A. R. McIsaac and W. Lin, *J. Am. Chem. Soc.*, 2015, **137**, 12241–12248.
21 S. S. Bao, G. K. H. Shimizu and L. M. Zheng, *Coord. Chem. Rev.*, 2019, **378**, 577–594.
22 C. Bloyet, J.-M. Rueff, J. Cardin, V. Caignaert, J.-L. Doualan, J.-F. Lohier, P.-A. Jaffrès and B. Raveau, *Eur. J. Inorg. Chem.*, 2018, 3095–3103.
23 R. M. P. Colodrero, P. Olivera-Pastor, E. R. Losilla, M. A. G. Aranda, L. Leon-Reina, M. Papadaki, A. C. McKinlay, R. E. Morris, K. D. Demadis and A. Cabeza, *Dalton Trans.*, 2012, **41**, 4045–4051.
24 M. T. Wharmby, J. P. S. Mowat, S. P. Thompson and P. A. Wright, *J. Am. Chem. Soc.*, 2011, **133**, 1266–1269.
25 B. P. Yang, A. V. Prosvirin, Y. Q. Guo and J. G. Mao, *Inorg. Chem.*, 2008, **47**, 1453–1459.
26 N. Hugot, M. Roger, J. M. Rueff, J. Cardin, O. Perez, V. Caignaert, B. Raveau, G. Rogez and P. A. Jaffrès, *Eur. J. Inorg. Chem.*, 2016, 266–271.
27 G. B. Hix, in *Metal Phosphonate Chemistry: From synthesis to application*, ed. A. Clearfield and K. Demadis, RSC Publishing, 2011, ch. 16, pp. 525–550.
28 J. M. Rueff, N. Barrier, S. Boudin, V. Dorcet, V. Caignaert, P. Boullay, G. B. Hix and P. A. Jaffrès, *Dalton Trans.*, 2009, 10614–10620.
29 B. Mutelet, S. Boudin, O. Perez, J. M. Rueff, C. Labbé and P. A. Jaffrès, *Dalton Trans.*, 2015, **44**, 1186–1192.
30 M. Berchel, T. Le Gall, C. Denis, S. Le Hir, F. Quentel, C. Elléouet, T. Montier, J. M. Rueff, J. Y. Salaün, J. P. Haelters, P. Lehn, G. B. Hix and P. A. Jaffrès, *New J. Chem.*, 2011, **35**, 1000–1003.
31 J. M. Rueff, O. Perez, V. Caignaert, G. Hix, M. Berchel, F. Quentel and P. A. Jaffrès, *Inorg. Chem.*, 2015, **54**, 2152–2159.
32 J. M. Rueff, G. B. Hix and P. A. Jaffrès, in *Tailored Organic–Inorganic Materials*, ed. E. Brunet, J. L. Colón and A. Clearfield, John Wiley & Sons, Inc., 1st edn, 2015, ch. 9, pp. 341–393, ISBN: 978-1-118-77346-8.
33 J. M. Rueff, O. Perez, A. Le Claire, H. Couthon-Gourvès and P. A. Jaffrès, *Eur. J. Inorg. Chem.*, 2009, 4870–4876.
34 J. M. Rueff, V. Caignaert, A. Leclaire, C. Simon, J. P. Haelters and P. A. Jaffrès, *CrystEngComm*, 2009, **11**, 556–559.
35 J. M. Rueff, O. Perez, A. Pautrat, N. Barrier, G. Hix, S. Hernot, H. Couthon-Gourvès and P. A. Jaffrès, *Inorg. Chem.*, 2012, **51**, 10251–10261.
36 Q. Evrard, Z. Chaker, M. Roger, C. M. Sevrain, E. Delahaye, M. Gallart, P. Gilliot, C. Leuvrey, J.-M. Rueff, P. Rabu, C. Massobrio, M. Boero, A. Pautrat, P.-A. Jaffrès, G. Ori and G. Rogez, *Adv. Funct. Mater.*, 2017, **27**, 1703576.
37 T. Basu, C. Bloyet, J. M. Rueff, V. Caignaert, A. Pautrat, B. Raveau, G. Rogez and P. A. Jaffrès, *J. Mater. Chem. C*, 2018, **6**, 10207–10210.
38 T. Basu, C. Bloyet, F. Beaubras, V. Caignaert, O. Perez, J. M. Rueff, A. Pautrat, B. Raveau, J. F. Lohier, P. A. Jaffrès, H. Couthon, G. Rogez, G. Taupier and H. Dorkenoo, *Adv. Funct. Mater.*, 2019, **29**, 19018783.
39 C. Bloyet, M. Roger, J. M. Rueff, B. Raveau, J. F. Lohier, G. Rogez and P. A. Jaffrès, *Eur. J. Inorg. Chem.*, 2016, 4643–4648.
40 J. M. Rueff, O. Perez, C. Simon, H. Couthon-Gourvès, C. Lorilleux and P. A. Jaffrès, *Cryst. Growth Des.*, 2009, **9**, 4262–4268.
41 P. O. Adelani, N. A. Martinez, N. D. Cook and P. C. Burns, *Eur. J. Inorg. Chem.*, 2015, 340–347.
42 J. Liang and G. K. H. Shimizu, *Inorg. Chem.*, 2007, **46**, 10449–10451.
43 H. L. Ngo, A. Hu and W. Lin, *J. Mol. Catal. A: Chem.*, 2004, **215**, 177–186.
44 G. A. Crosby, R. G. Highland and K. A. Truesdell, *Coord. Chem. Rev.*, 1985, **64**, 41–52.
45 R. G. Highland, J. G. Brummer and G. A. Crosby, *J. Phys. Chem.*, 1986, **90**, 1593–1598.
46 K. J. Jordan, K. A. Wacholtz and G. A. Crosby, *Inorg. Chem.*, 1991, **30**, 4588–4593.
47 N. M. Avram and M. G. Brick, *Optical Properties of 3d-Ions in Crystals*, Springer, Berlin, 2013.
48 D. T. Palumbo and J. J. Brown Jr., *J. Electrochem. Soc.*, 1970, **117**, 1184–1188.
49 H. Souissi and S. Kammoun, *Mater. Sci. Appl.*, 2011, **2**, 1121–1126.
50 B.-S. Bae and M. C. Weinberg, *J. Non-Cryst. Solids*, 1994, **168**, 223–231.
51 L. Palatinus and G. Chapuis, Superflip - a computer program for the solution of crystal structures by charge flipping in arbitrary dimensions, *J. Appl. Crystallogr.*, 2007, **40**, 786–790.
52 G. Oszlanyi and A. Suto, Ab initio structure solution by charge flipping, *Acta Crystallogr., Sect. A: Found. Crystallogr.*, 2004, **60**, 134–141 or ShelXS. G. M. Sheldrick, *Acta Crystallogr., Sect. A: Found. Crystallogr.*, 2008, **64**, 112–122.
53 V. Petříček, M. Dušek and L. Palatinus, *Z. Kristallogr. – Cryst. Mater.*, 2014, **229**, 345.
54 O. V. Dolomanov, L. J. Bourhis, R. J. Gildea, J. A. K. Howard and H. Puschmann, *J. Appl. Crystallogr.*, 2009, **42**, 339–341.
55 P. A. Jaffrès, N. Bar and D. Villemin, *J. Chem. Soc., Perkin Trans. 1*, 1998, 2083–2089.

56 P. Tavs, *Chem. Ber.*, 1970, **103**, 2428.
57 C. M. Sevrain, M. Berchel, H. Couthon and P. A. Jaffrès, *Beilstein J. Org. Chem.*, 2017, **13**, 2186–2213.
58 A. Le Bail, *Powder Diffr.*, 2005, **20**, 316–326.
59 A. Boultif and D. Louer, *J. Appl. Crystallogr.*, 2004, **37**, 724–731.
60 J. Rodriguez-Carvajal, *Phys. B*, 1993, **192**, 55.
61 J. T. Culp, G. E. Fanucci, B. C. Watson, A. N. Morgan, R. Backov, H. Ohnuki, M. W. Meisel and D. R. Talham, *J. Solid State Chem.*, 2001, **159**(2), 362–370.
62 M. E. Lines, *J. Phys. Chem. Solids*, 1970, **31**(1), 101–116.
63 S. G. Carling, G. E. Fanucci, D. R. Talham, D. Visser and P. Day, *Solid State Sci.*, 2006, **8**(3), 321–325.
64 G. E. Fanucci, J. Krzystek, M. W. Meisel, L.-C. Brunel and D. R. Talham, *J. Am. Chem. Soc.*, 1998, **120**(22), 5469–5479.
65 S. G. Carling, P. Day, D. Visser and R. K. Kremer, *J. Solid State Chem.*, 1993, **106**, 111–119.
66 S. G. Carling, P. Day and D. Vissen, *Inorg. Chem.*, 1995, **34**(15), 3917–3927.
67 R. L. Carlin, *Magnetochemistry*, Springer-Verlag, Berlin, 1986.
68 R. Navarro, *Magnetic Properties of Layered Transition Metal Compounds*, Kluwer Academic Publishers, Dordrecht, 1990.
69 P. Rabu, P. Janvier and B. Bujoli, *J. Mater. Chem.*, 1999, **9**, 1323–1326.
70 C. Bellitto, E. M. Bauer and G. Righini, *Coord. Chem. Rev.*, 2015, **289–290**, 123–136.
71 P. W. Thulstrup, L. Broge, E. Larsena and J. Springborga, *Dalton Trans.*, 2003, 3199–3204.
72 S. Chandra and L. K. Gupta, *Spectrochim. Acta, Part A*, 2004, **60**, 1751–1761.
73 J. Braz, *Chem. Soc.*, 2015, **26**, 2607–2614.
74 J. Krausko, J. K. Malongwe, G. Bičanova, P. Klan, D. Nachtigallova and D. Heger, *J. Phys. Chem. A*, 2015, **119**, 8565–8578.
75 D. T. Palumbo and J. J. Brown Jr., *J. Electrochem. Soc*, 1970, **117**, 1184–1188.
76 H. Souissi and S. Kammoun, *Mater. Sci. Appl.*, 2011, **2**, 1121–1126.
77 B.-S. Bae and M. C. Weinberg, *J. Non-Cryst. Solids*, 1994, **168**, 223–231.
78 M. Kawano, H. Takebe and M. Kuwabara, *Opt. Mater.*, 2009, **32**, 277.
79 J. Braz, *Chem. Soc.*, 2015, **26**(12), 2607–2614.
80 Z. C. Liu, Z. Y. Yang, T. R. Li, B. D. Wang, Y. Li, D. D. Qin, M. F. Wang and M. H. Yan, *Dalton Trans.*, 2011, **40**, 9370–9373.
81 R. Krämer, *Angew. Chem., Int. Ed.*, 1998, **37**, 772–773.
82 G. Nagarjuna, *et al.*, *Solid State Commun.*, 2010, **150**, 9–13.